# Probabilistic cell seeding and non-autofluorescent 3D-printed structures as scalable approach for multi-level co-culture modeling

Sebastian Buchmann [a,b,1], Alessandro Enrico [c,d,1], Muriel Alexandra Holzreuter [b,c], Michael Reid [e], Erica Zeglio [a,b], Frank Niklaus [c,***], Göran Stemme [c,**], Anna Herland [a,b,*]

[a] *Division of Nanobiotechnology, KTH Royal Institute of Technology, Tomtebodavägen 23a, 171 65, Solna, Sweden*
[b] *AIMES – Center for the Advancement of Integrated Medical and Engineering Sciences, Department of Neuroscience, Karolinska Institute, 17177, Stockholm, Sweden*
[c] *Division of Micro and Nanosystems, KTH Royal Institute of Technology, Malvinas väg 10, 100 44, Stockholm, Sweden*
[d] *Synthetic Physiology lab, Department of Civil Engineering and Architecture, University of Pavia, Via Ferrata 3, 27100, Pavia, Italy*
[e] *Department of Fiber and Polymer Technology, Wallenberg Wood Science Centre, KTH Royal Institute of Technology, Teknikringen 56-58, 100 44, Stockholm, Sweden*

## ARTICLE INFO

## ABSTRACT

To model complex biological tissue in vitro, a specific layout for the position and numbers of each cell type is necessary. Establishing such a layout requires manual cell placement in three dimensions (3D) with micrometric precision, which is complicated and time-consuming. Moreover, 3D printed materials used in compartmentalized microfluidic models are opaque or autofluorescent, hindering parallel optical readout and forcing serial characterization methods, such as patch-clamp probing. To address these limitations, we introduce a multi-level co-culture model realized using a parallel cell seeding strategy of human neurons and astrocytes on 3D structures printed with a commercially available non-autofluorescent resin at micrometer resolution. Using a two-step strategy based on probabilistic cell seeding, we demonstrate a human neuronal monoculture that forms networks on the 3D printed structure and can establish cell-projection contacts with an astrocytic-neuronal co-culture seeded on the glass substrate. The transparent and non-autofluorescent printed platform allows fluorescence-based immunocytochemistry and calcium imaging. This approach provides facile multi-level compartmentalization of different cell types and routes for pre-designed cell projection contacts, instrumental in studying complex tissue, such as the human brain.

## 1. Introduction

To fully recapitulate the complexity of human organs and tissues, multiple cell populations must be precisely organized in all three dimensions, something that is impossible in models based on random 2D cultures and 3D cell-laden hydrogels. [1–6] Conventional two-dimensional (2D) cell culture models are a simple and powerful tool for studying cellular mechanisms. However, the limited dimensionality and spatial control over the cell positioning make them insufficient to study medium- and high-complexity tissue processes, such as defined neuronal-astrocyte interactions and the blood-brain barrier (BBB). [7] 3D hydrogels with encapsulated cells provide an *in vivo*-like environment, but these models typically feature a random distribution of cells in the hydrogel. This lack of spatial definition for interconnections between cells limits the complexity and reproducibility of 3D cell interactions. [8] While cell migration and scaffold invasion can be guided by inducing a gradient of growth factors or chemotactic compounds, these processes take days to occur. In addition, thick 3D models require gas and nutrient transport solutions to avoid tissue necrosis. [9,10] All these elements make current 3D modeling solutions complex, expensive, and often too undefined to mimic tissue physiology.

Compartmentalization strategies based on microfluidic systems tackle part of these issues. [11] Advances in microfluidics and 3D printing enabled organ-on-a-chip technologies where cells can be cultivated in controlled microenvironments with integrated sensors or can be placed using extrusion printing. [12–21] For instance, microchannels can guide

---

* Corresponding author. Division of Nanobiotechnology, KTH Royal Institute of Technology, Tomtebodavägen 23a, 171 65, Solna, Sweden.
** Corresponding author. Division of Micro and Nanosystems, KTH Royal Institute of Technology, Malvinas väg 10, 100 44, Stockholm, Sweden.
*** Corresponding author. Division of Micro and Nanosystems, KTH Royal Institute of Technology, Malvinas väg 10, 100 44, Stockholm, Sweden.
*E-mail addresses:* frank@kth.se (F. Niklaus), stemme@kth.se (G. Stemme), aherland@kth.se (A. Herland).
[1] These authors contributed equally.

the growth of neurites to study axonal regeneration and neuronal communication. [22–24] Fabrication methods such as soft lithography and injection molding can quickly generate 2.5D guiding structures. However, these methods are still too complicated and expensive to fabricate overhanging and multi-level microstructures that resemble the physiological microenvironment. Recently, two-photon polymerization has been used to generate 3D microscaffolds for neurite guidance, providing a solution to obtain 3D environments where the position and connection points of cells are defined with micrometric accuracy. [25,26] However, these examples used nanoliter handling methods for manual biofunctionalization, cell seeding, or cell interrogation, making these solutions complicated and time-consuming. In addition, the intrinsic autofluorescence of most of the available photopolymerizable resins for 3D printing hinders standard imaging techniques in these 3D-printed micro scaffolds. [27]

To address the limitations of current 3D models based on two-photon 3D-printed scaffolds, we developed a multi-level co-culture model using a low-autofluorescent polymer and a parallel yet statistically selective seeding approach (Fig. 1a). We used a probabilistic two-step approach to seed astrocytes first and then neurons, yielding defined neuronal-astrocytic interactions without requiring selective coatings or positioning of individual cells (Fig. 1b). The protocol uses different seeding time points and densities for the two cell types to enable only neurons on top of the 3D printed structures and a 2D co-culture of neurons and astrocytes on the underlying glass substrate (Fig. 1c). Dedicated neurite guidance structures (ramps) also define the interaction pathways between the neurons and the astrocytes, allowing the investigation of how

contact-mediated and biochemical signaling shape the interactions between the two cell types. Since the transparent printed structures display little to no autofluorescence, the co-culture model can be characterized using high-throughput, non-contact fluorescence microscopy even with low-signal assays, such as calcium imaging in neurons or single-molecule fluorescence. As proof of concept, we examined neuronal protein expression by immunocytochemistry and electrophysiological activity by fluorescent calcium imaging (Fig. 1d). [28,29]

## 2. Results and discussion

### 2.1. Design, optimization, and characterization of the printed structures

We demonstrate a multi-level co-culture system with geometrically defined neuronal-astrocytic interaction points and neurite guidance using a 3D printed platform (Fig. 1a). To fabricate the 3D platform, a commercially available two-photon 3D printer (Nanoscribe GT2, Nanoscribe, Germany) was used to print 3D solid structures in a low-autofluorescent, methacrylate-based, biocompatible resin (IP-Visio, Nanoscribe, Germany) on ITO-coated glass substrates using two-photon polymerization (see Experimental section for detail). The 3D printed structure consists of $4 \times 2$ micropillars with narrow suspended bridges connecting the pillars (Fig. 2a–b, see Experimental section for the detailed design description). The optimization of the printing parameters and the characterization of stiffness and surface charge using Atomic Force Microscopy (AFM) and Colloidal Probe AFM (CP-AFM) can be found in the Supplementary Material (Figs. S1 and S2). [30] Each pillar
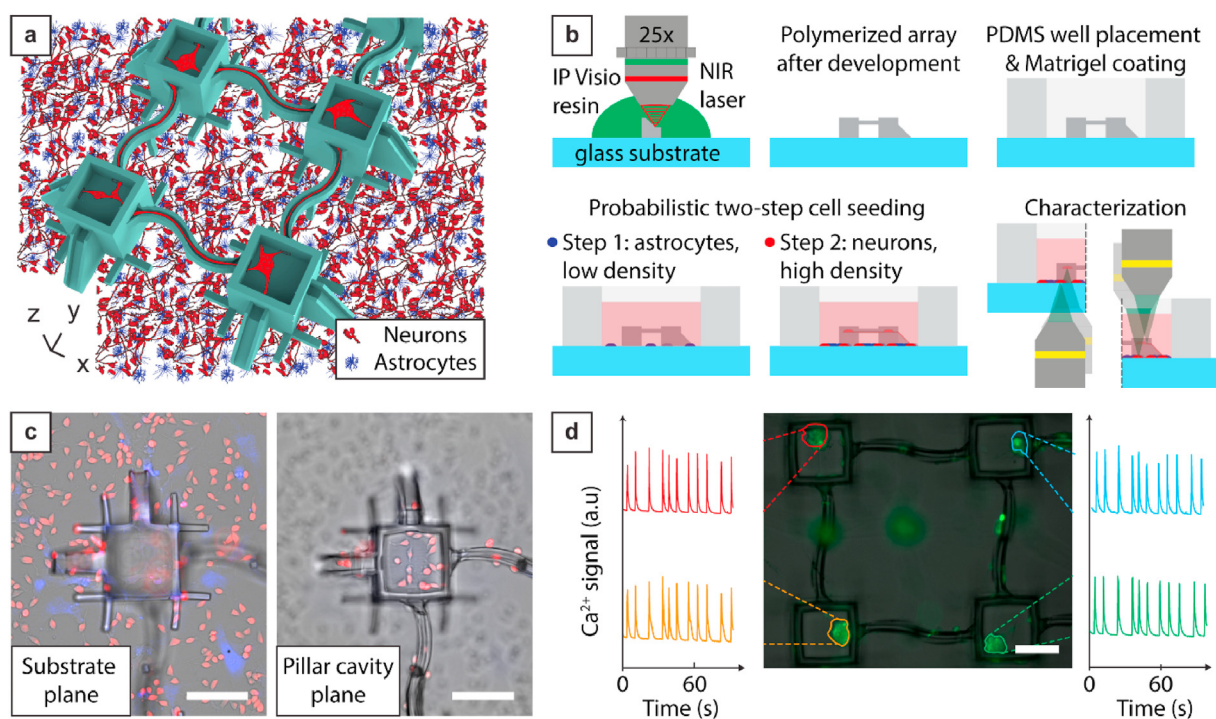


**Fig. 1. Scalable approach for parallel seeding and characterization of neuronal-astrocytic co-culture models.** a) Schematic illustration (side view) of the co-culture model. Neurons (red) and astrocytes (blue) cover the glass substrate surface. The elevated 3D printed structures (in green) feature only seeded neurons, forming connections between the neuronal population on the 3D printed pillar cavities and the co-culture population on the glass substrate surface through the ramps connecting the glass substrate surface and the cavity on top of the pillar. b) Process flow for the realization of the co-culture models. A commercially available low-autofluorescent resin, IP Visio, is printed using a $25 \times 0.8$ NA objective lens in resin immersion configuration. After development, a PDMS well is placed on the glass substrate. After Matrigel® coating, we first seeded astrocytes with low density, cultured the cells to reach confluency, and then seeded neurons with high density to obtain two levels with different cell populations. The transparency of the substrate and resins allow both upright and inverted microscopy characterizations. c) Fluorescence images (substrate and pillar cavity planes) of the 3D printed structures after two-step cell seeding. The blue and red cell tracker colors visualize the presence of astrocytes and neurons, respectively. The glass substrate plane image shows a co-culture of neurons and astrocytes, while only neurons are present on top of the structures (pillar cavity plane). Scales bars, 100 μm. d) Indirect visualization of electrophysiological activity of neurons by calcium imaging recorded with an inverted wide-field microscope. Each recording site is indicated with dashed lines in the pillar cavity. Scales bar, 100 μm. (For interpretation of the references to color in this figure legend, the reader is referred to the Web version of this article.)
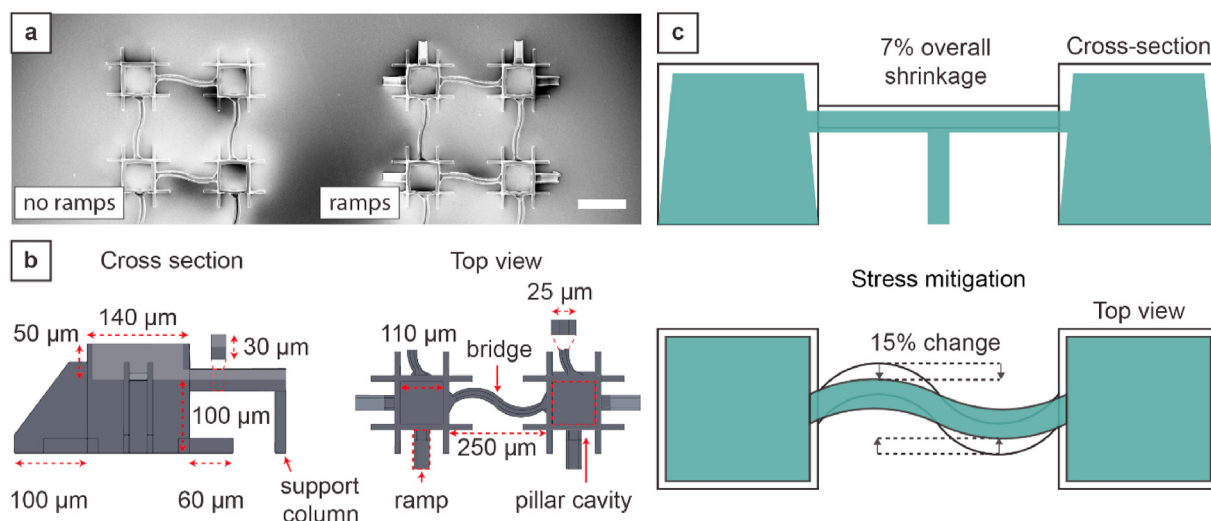
**Fig. 2. Design, optimization, and characterization of the printed structures.** a) SEM image (top view) showing the printed platform composed of two pillar arrays with and without ramps connecting the pillar cavities with the substrate. Scale bar, 200 μm. b) 3D model of the structures with nominal dimensions. c) Illustration of post-printing structure shrinkage. The values are based on comparing the dimensions and distances of the 3D model with the measurements in SEM images of printed structures.

top is designed with a cavity to host cells (neurons in this study) and to prevent them from migrating to other areas after cell seeding and adhesion. The cells seeded into the pillar cavities are 100 μm above the substrate plane and can be distinguished from those on the substrate without significant optical crosstalk, even using wide-field microscopy. Suspended bridges connect all the cavities in the pillar arrays to guide the neurite growth and formation of a network on top of the printed structures.

To allow detailed contact vs. non-contact assays of cell behavior, we printed two copies of the array per sample and included dedicated structures (ramps) in one of the copies to connect the cavities to the glass substrates (Fig. 2a). The ramps define specific pathways for physical contact between the neurons inside the pillar cavities and the co-culture of neurons and astrocytes on the underlying substrate. This approach thus enables the precise organization of two separated cell culture planes.

To avoid the delamination of the 3D-printed structures after development, we combined a chemical treatment of the substrate and stress relief features in the design of the structures. A challenge when printing microstructures with a millimetric footprint is to avoid mechanical failure due to post-printing shrinkage. Many two-photon polymerization resins suffer from a significant post-printing shrinkage (5–10%), which is also present for the type of resin used in this study (Fig. 2c). [31,32] The shrinkage causes mechanical stress in the structures that tend to delaminate from the substrate if there is no strong adhesion between resin and substrate or stress relaxation feature. To improve the adhesion between the glass substrate and the printed resin, we chemically modified the ITO-coated glass substrate with the silane 3-(trimethoxysilyl)propyl methacrylate (see Experimental section). Then, we optimized the design to counteract the stress build-up after printing. Specifically, we designed the connections between the pillars as thin serpentine-shaped flexible bridges that could absorb the tensile stress by straightening them out after printing, avoiding the delamination of the entire structure from the glass substrate. These connections are long and unsupported structures, which increases the risk of stitching-induced printing error due to the sinking or deformation of the structures after printing. We included a support column in the midpoint between pillars to mitigate this issue. The amplitude of the sinusoidal shape of the connection is reduced by roughly 30% after printing, indicating that the stress is released as intended with the deformation of the thin bridges and does not build up between pillars (Fig. 2c). Previous studies featuring two-photon

polymerized platforms presented a similar solution by printing a large block as a base and a spring connecting the block to the glass substrate. [26,27] However, a millimeter-sized 3D printed structure significantly increases the printing time (by a factor of 2–10) and prevents conventional inverted imaging during cell culture and final assessments. Instead, our configuration, combined with the printed structures' transparency, allows conventional inverted microscopy for cell imaging and characterization (Fig. 1c and d) – a significant advantage with respect to previous methods. [27]

### 2.2. Neurite outgrowth guided by the 3D printed platform

To verify that the 3D printed platform works as a suitable scaffold for neurons, we used Lund human mesencephalic (LUHMES) cells as a human neuronal model, observing the formation of neurites along the printed structures. LUHMES cells are frequently chosen to perform toxicity assays and Parkinson's disease modeling due to their rapid differentiation into post-mitotic neurons with characteristics of dopaminergic neurons [33,34]. To promote neuronal adhesion and growth, we tested three substrate treatments: poly-L-ornithine (PLO) coating with fibronectin and laminin, PLO with fibronectin, or Matrigel® coating (see Table S1 in the Supplementary Material). LUHMES cells were typically differentiated for 9–12 days. [33,35] In this study, we observed that the density of LUHMES cells on substrates coated with PLO/fibronectin or with PLO/fibronectin/laminin would drastically decrease between differentiation days 5 and 9. We then evaluated Matrigel®, resulting in significantly better support for LUHMES cell adhesion and neurite outgrowth on top of printed structures. Using Matrigel® as substrate coating, LUHMES cells formed neurite networks on the ITO-coated glass substrate and the 3D-printed resin. Through their neurite extensions, neurons inside the pillar cavities can physically connect to the neurons on the other pillars and to co-cultured cells on the glass substrate if ramps are present (Fig. 3a). However, without the ramp structure, the neurons on the pillars without ramps remain physically isolated from the co-culture (Fig. 3b). The neurons could also attach and grow on the outer wall of the pillars and suspended bridges, extending to the bottom substrate. No significant autofluorescent signal from the 3D-printed structures could be detected under normal microscopy conditions, simplifying confocal imaging of the networks (Fig. S3 in the Supplementary Material).
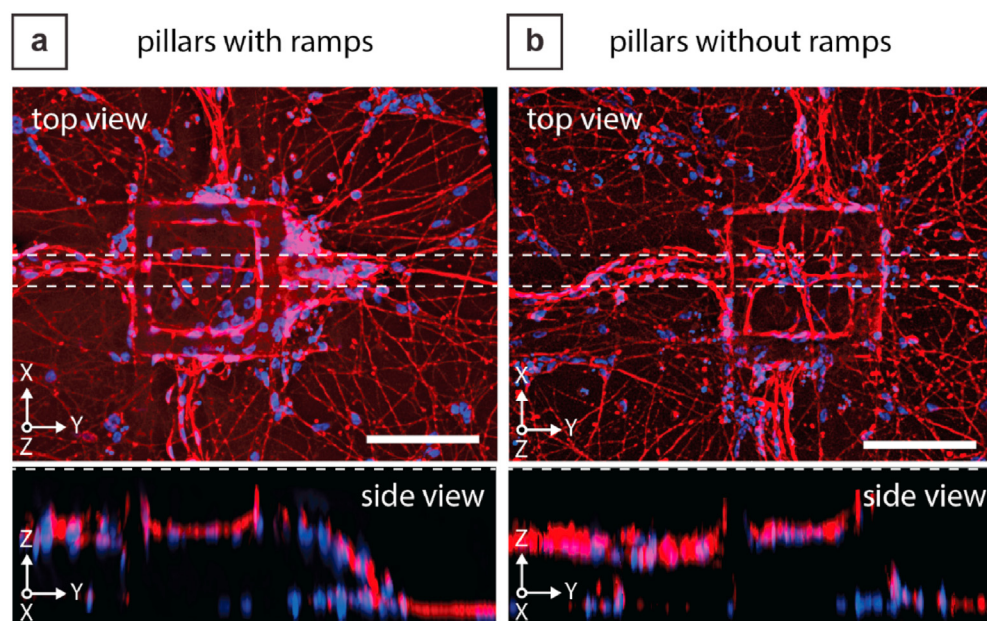
**Fig. 3. Neurite outgrowth guided by the 3D printed structure.** Confocal images (top view and cross-sectional view) of pillar cavities populated with differentiated LUHMES cells (day 8) for pillars a) with and b) without ramp connection, showing how neurites extend down the ramps or are isolated inside the pillar cavities based on the presence or absence of the ramp structure, respectively. Samples stained with anti-TUBB3 (red) and Hoechst/Nuclei (blue). The images on the lower panel show the side view of the areas highlighted with a white dashed line in the images of the upper panel. Scales bars, 100 μm. (For interpretation of the references to color in this figure legend, the reader is referred to the Web version of this article.)

### 2.3. Probabilistic two-step cell seeding for scalable compartmentalization

To avoid serial and time-consuming cell positioning via patch-clamp-like nanoliter pipetting, we developed a seeding protocol to obtain a neuron-only population on the top of the printed structures and a co-culture of neurons (i.e., LUMHES) and astrocytes on the substrate plane (Fig. 4a). To visualize the outcome of this approach, we stained the two cell populations with different fluorescent dyes before seeding. First, we seeded human cortical astrocytes at a low density (2500 cells/cm$^2$). The area on top of the individual pillar (0.012 mm$^2$) was chosen to allow the spread and growth of multiple neurons inside the pillar cavities while minimizing the probability of astrocytes landing in the pillar cavities when seeded with low cell density (Fig. 4b and **c**). After one day of culture, we found an average of 1.89 ± 0.16 astrocytes inside each 2 × 4 array (based on brightfield counting on 102 2 × 4 pillar arrays). This number aligns with the theoretical value (2.4), which we calculated assuming a uniform distribution of the seeded cells per unit area, considering the total area of the eight pillar cavities, and no loss due to viability or delamination. The number of cells (10–15 cells covering 2% of the region of interest, consisting of an area of 0.005 cm$^2$) we identify on the substrate also matches the expected value based on the low seeding density. We first cultured the astrocytes in astrocyte media to allow proliferation and increase their area coverage (Fig. 4d and **e**). Three days after seeding, no additional astrocyte was found on top of the structures, while the number of cells on the substrate grew to roughly 40–50 with a 10% area coverage. Before seeding the neurons, we identified the pillar cavities containing astrocytes and excluded them from further analysis. Once the astrocytes reached 10% confluency, we first replaced the astrocyte media with LUHMES differentiation media and then seeded LUHMES cells at high cell density (150000 cells/cm$^2$), populating both the substrate plane and the pillar cavities (Fig. 4f and **g**). 4 h after seeding, we found an average of 11.4 ± 3.7 cells inside each pillar cavity (based on brightfield counting on 184 pillars). With this two-step seeding approach, we obtain observable neurons in three distinct conditions: 1) neurons inside the pillar cavities without ramps, physically isolated from the astrocytes but within proximity to the astrocyte-neuron co-culture from the bottom substrate layer, 2) neurons inside the pillar cavities with ramps connection, which can connect to the astrocyte-neuron co-culture through neurite extensions, and 3) neurons that grow in direct physical contact on top of the astrocytes on the bottom substrate layer. This setup can be used to study the effect of contact-mediated interactions (direct or through neurites) compared to the indirect interaction through extracellular biochemical signaling.

### 2.4. Structure biocompatibility and optimization of the cell culture protocol

To verify the compatibility of the 3D-printed structures with the two cell populations, we run multiple viability assays. Qualitative image analysis of the cell density showed equal distribution on the substrate next to the printed structures and farther away from them. We then performed a quantitative evaluation of the cell viability using a live-dead assay. LUHMES cells (differentiation day 9) in co-culture with human astrocytes had comparable viability in control well plates and in the presence of the printed structures, indicating that the printed structures are biocompatible and do not leach out cytotoxic chemicals during the multiday cell culture (Fig. 5a). We then examined the viability of LUHMES cells as monoculture and co-cultured with astrocytes. The viability of LUHMES and human astrocyte cells in co-culture decreased significantly compared to LUHMES differentiated as a monoculture (Fig. 5b). The low viability was associated with little to no neurite outgrowth, likely because the LUHMES cells did not properly differentiate into post-mitotic neurons. Previous toxicological studies instead reported beneficial effects for LUHMES cells when co-cultured with immortalized or embryonic stem cell-derived mouse astrocytes. [36,37] Our contradicting results indicate that the combination of LUHMES-derived neurons and human cortical astrocytes is sub-optimal for co-culture models, highlighting the non-trivial interplay between the specific cell models used in co-culture studies. To understand the source of this discrepancy, we first examined the viability of primary human astrocytes in different media conditions (Fig. S4 in the Supplementary Material). Since the viability of astrocyte monocultures did not decrease significantly when astrocyte monocultures were kept in differentiation media, we hypothesized that biological stress arises during the high-density seeding of LUHMES cells on top of the astrocyte cell layer. This stress can cause a direct reduction in the viability of the co-culture and a neurotoxic response from the astrocytes, further decreasing the viability. [38] To minimize the stress reaction, we changed the culture media composition after LUHMES seeding from standard differentiation media (DM) to a modified version (DM+) by including astrocyte growth factor supplements and ROCK inhibitor. Seeding LUHMES cells in DM + culture conditions significantly increased the viability of the co-culture (Fig. 5c). The adapted media allowed us to co-culture the human
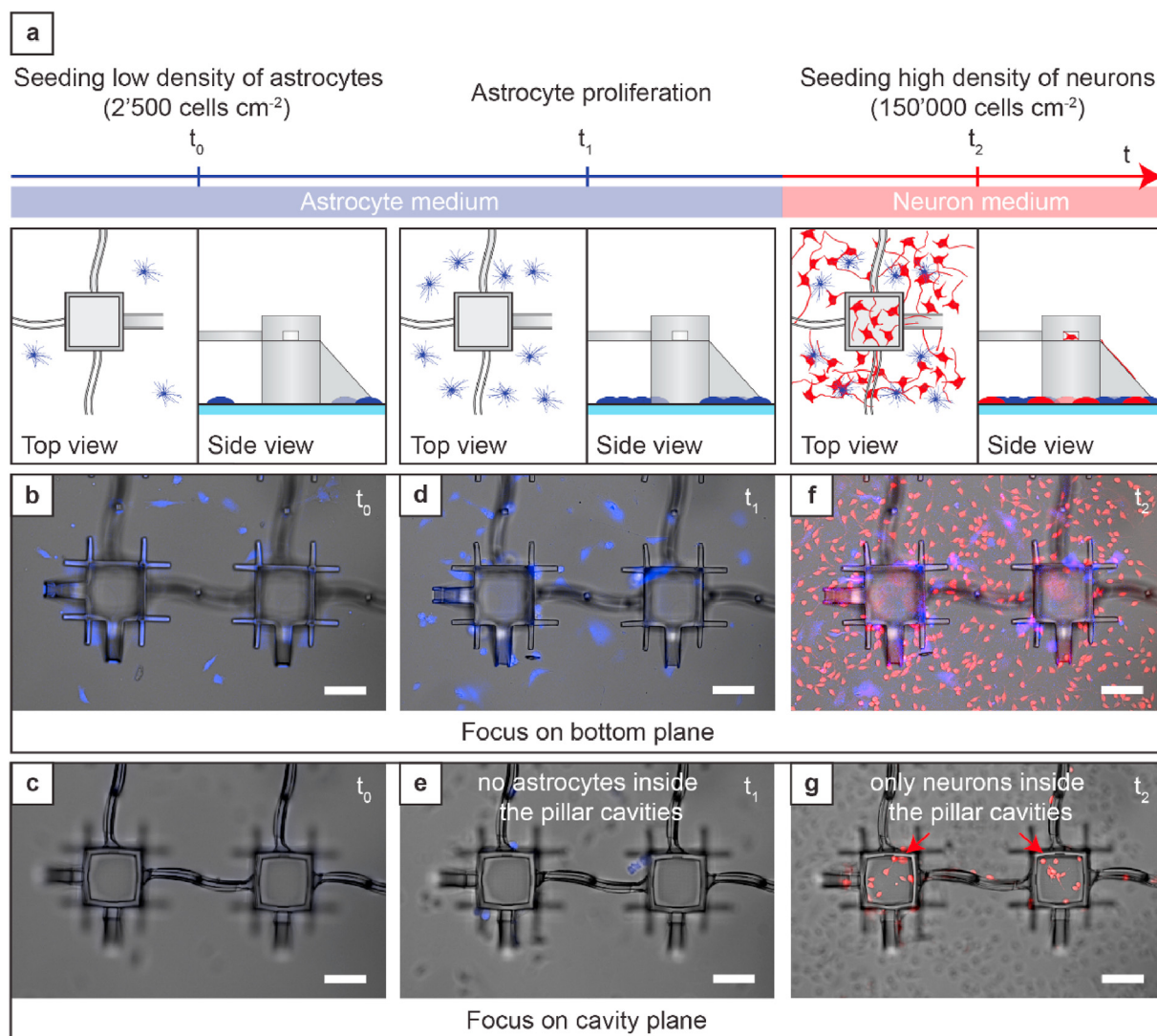
**Fig. 4. Two-step seeding approach to generate neuronal monoculture inside the pillar cavities and astrocytes-neurons co-culture on the substrate surface.**
a) Schematic illustration of the two-step seeding method. Astrocytes (in blue) are first introduced with a low seeding density (2500 cells/cm$^2$) not to get astrocytes in the pillar cavities. Next, the astrocytes are cultured until they reach the desired level of confluency. Then, neurons (in red) are seeded with high-cell density (150000 cells/cm$^2$) populating the substrate, forming a co-culture with the astrocytes. The pillar cavity features neuronal populations isolated from the underlying co-culture or confined contact points in the presence of the ramps. Figures b) to g) are top-view microscopy images composed using the brightfield signal and the fluorescence signal from the cell tracker dyes (top view). b) Astrocytes (blue cells) on the glass substrate 2 h after astrocyte seeding. The initial area coverage on the glass substrate is low (around 2%), in line with the low seeding density, and increases over time, reaching around 10% in d). f), g) Neurons (red cells) 4 h after neuron seeding. No astrocytes are found on top of the structures at any stage (c, e, g). Scale bars, 100 μm. (For interpretation of the references to color in this figure legend, the reader is referred to the Web version of this article.)

astrocytes and LUHMES cells to obtain post-mitotic neurons showing neurite extensions and maturing electrophysiological properties.

### 2.5. Protein expression analysis

After optimizing the co-culture protocol, we assessed the influence of human astrocytes on the differentiation process of the LUHMES cells. The co-culture platform allows performing fluorescent imaging directly through the printed structures, thus enabling investigation of the protein expression of LUHMES cells differentiating inside the pillar cavities (with and without ramps) using immunocytochemistry with standard microscopy. Therefore, we evaluated the protein expression of tyrosine hydroxylase (TH, a marker for dopaminergic neurons), synapsin 1 (SYN1, a presynaptic marker), and doublecortin (DCX, a microtubule-associated protein). All three proteins show increased expression in differentiated LUHMES cells and are used as maturity markers. [33,39,40] The

quantitative analysis showed that TH is significantly downregulated in all co-culture conditions (LUHMES cells growing on the bottom substrate layer and inside pillar cavities) compared to the monoculture (Fig. 6a). However, TH was equally expressed in the differentiated LUHMES monoculture growing on the bottom substrate layer and inside the pillar cavities (with and without ramps), indicating that the printed structure did not affect TH expression (Fig. 6b). Furthermore, we measured no significant difference in TH expression in the co-culture samples between 1) the neurons on the bottom substrate layer where they grow in direct contact on top of the astrocytes, 2) the neurons growing inside the pillar cavities without ramps and thus without direct physical contact with astrocytes, and 3) the neurons growing inside the pillar cavities with ramps that allow them to connect with the astrocytes co-culture through neurite extensions growing down the ramps (Fig. 6c). These results indicate that the downregulation in the LUHMES cells, when co-cultured with astrocytes, is mainly caused by biochemical signaling, not
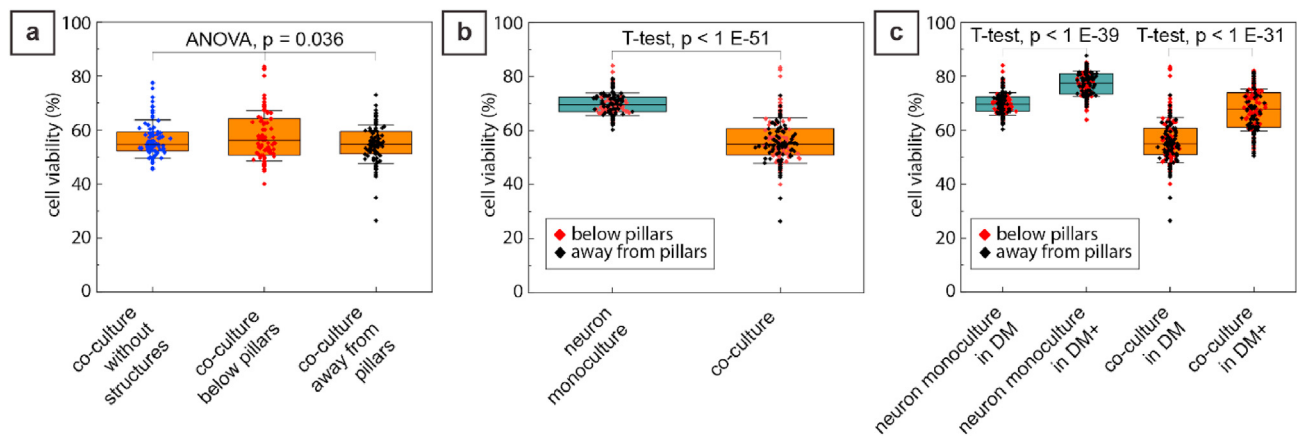
**Fig. 5. Viability assay and optimization of the co-culture models.** a) Viability analysis co-culture of LUHMES cells (differentiation day 9) and human astrocytes in a conventional well plate with no printed structures (control) and in the PDMS well close (<1 mm) and far (>2 mm) from the printed structure. No significant difference in viability was found, indicating good biocompatibility of the printed structures. b) Viability assay of differentiated LUHMES cells as monoculture and co-culture with human astrocytes. We found the viability of the co-culture to be significantly lower (p«0.005), suggesting a loss of viability due to the high cell density seeding. c) Cell culture protocol with the optimized co-culture protocol (DM+). Supplementing standard (DM) differentiation media with ROCK inhibitor and astrocyte growth factor supplement significantly increases the viability of both neuron monocultures and neuronal-astrocytic co-cultures (p«0.0005). One-way ANOVA test and two-sample *t*-test were performed to obtain the p values. Error bars show the standard deviations, with the centerline being the median value, and box plots corresponding to 25 and 75 percentiles.
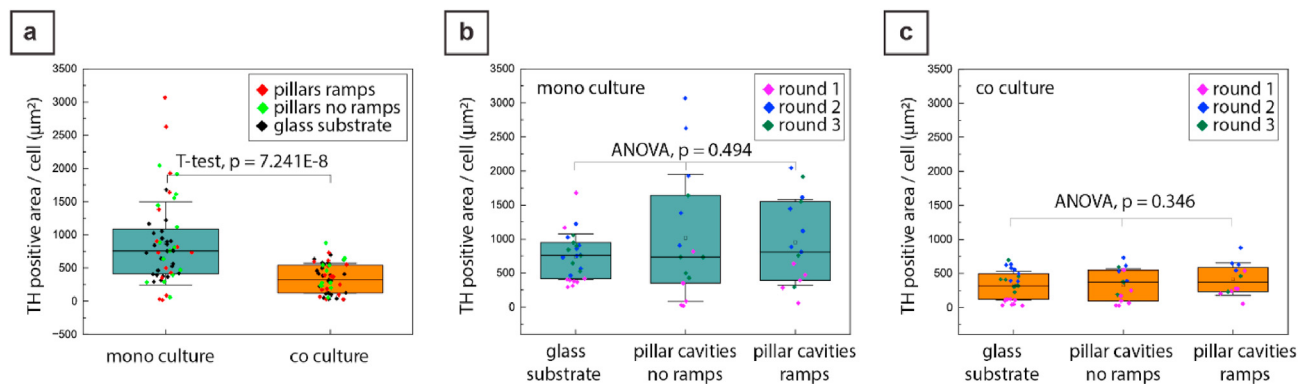


**Fig. 6. TH Protein expression.** ICC-based TH protein expression analysis in a) differentiated LUHMES cells from monoculture and in co-culture with human astrocytes showing downregulation of TH in the co-culture condition, b) TH expression in LUHMES cells differentiated inside the printed pillar cavities and on the bottom substrate layer showing similar expression, and c) TH expression in LUHMES cells differentiated in co-culture condition with human astrocytes growing on the substrate layer directly on top of the astrocytes or inside the pillar cavities with and without ramp connection to the astrocyte co-culture. One-way ANOVA test and two-sample *t*-test were performed to obtain the p values. Error bars show the standard deviations, centerline the median value, and box plots 25 and 75 percentiles.

contact-mediated. Furthermore, comparing the expression of SYN1 and DCX genes showed no significant difference in differentiated LUHMES cells grown as monoculture or in co-culture with the astrocytes (Fig. S5 in the Supplementary Material). Previous studies showed that astrocytes have a neuroprotective mechanism for dopaminergic neurons, [36,41, 42] increase the TH expression in neurons, [43–45] and promote synapse formation. [46,47] Comparable protein expression values in monocultures and co-cultures suggest that the human fetal cortical astrocytes used in this study do not support the maturation of LUHMES cells.

### 2.6. Indirect study of cell electrophysiology by calcium imaging

Thanks to the transparent printing resin, we could use our platform for live calcium imaging to investigate the electrophysiological properties of the neurons instead of using the time-consuming and more invasive patch-clamp method. Moreover, the absence of a significant fluorescence background simplifies the quantitative comparison of protein expression and calcium oscillations for the two spatially separated cell populations. Similar to the protein expression investigation, we aimed to investigate if contact-mediated or biochemical signaling-based

interactions between astrocytes and neurons influence the electrophysiological property of the neurons. It has been shown that astrocytes modulate the electrophysiological properties of neurons and help to increase the spontaneous firing activity of action potentials and speed up the maturation process. [48–50] Differentiated LUHMES cells showed spontaneous calcium activity cultured as monoculture and co-culture, but the calcium fluctuations from the cells were too small to compare cell behavior in the different conditions quantitatively.

To verify the compatibility of the printed structures with low-signal imaging scenarios, we used a well-established rodent model - rat neurons and rat astrocytes - with the optimized seeding protocol. [50] The rat cells formed neuronal networks on the printed structures. The calcium waves from the rat neurons produced strong signals that could be easily quantified (Fig. 7a). We cultured rat neurons as monoculture or co-culture with rat astrocytes for 21 days and then compared the neuronal firing rates using fluorescent calcium imaging. Monocultures of rat neurons showed comparable spontaneous activity, independent of the neurons' substrate (pillar cavities or glass substrate, Fig. 7b). This result confirms that, despite neurons inside the pillar cavities having fewer options to form a network than those on the substrate layer, the
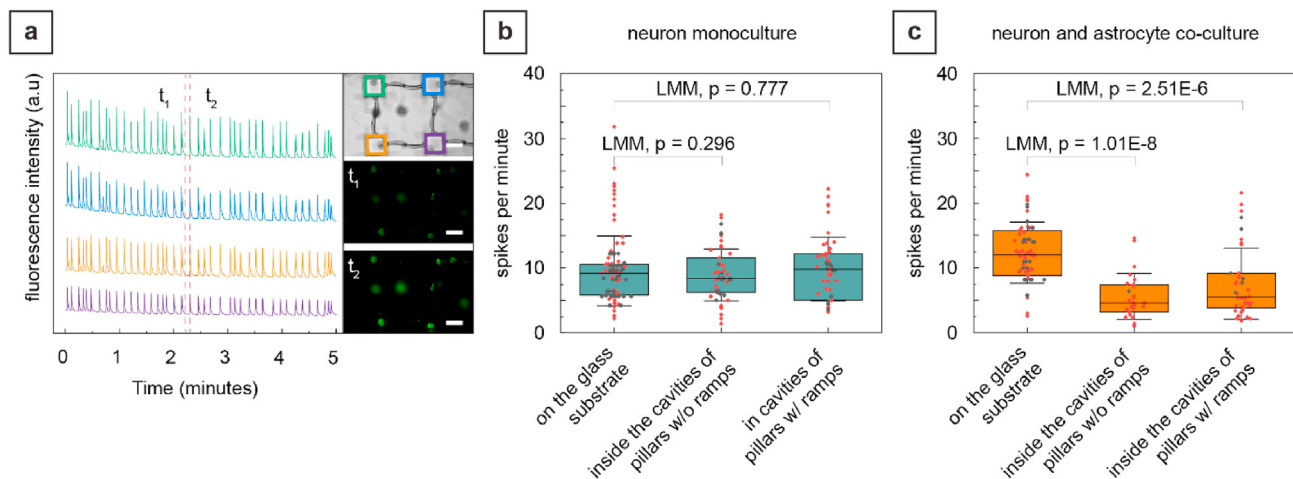
**Fig. 7. Calcium imaging of rat neurons and rat astrocytes.** a) Calcium imaging of isolated neuron population growing inside the pillar cavities (green calcium dye Calbryte™ 520 AM). Scale bars, 100 μm. b) Characterization of the spontaneous firing rate of rat neuron monocultures on the glass substrate layer and inside the pillar cavities with and with our ramps. c) Characterization of the spontaneous firing rate of rat neurons in co-culture with rat astrocytes, growing on the substrate layer directly on top of the astrocytes or inside the pillar cavities with and without ramp connection to the astrocyte co-culture. P values were calculated using Linear Mixed Models. Red and black marked data points represent two experimental rounds (see Fig. S6b and materials and method section). Error bars show the standard deviations, centerline the median value, and box plots 25 and 75 percentiles. (For interpretation of the references to color in this figure legend, the reader is referred to the Web version of this article.)

3D-printed structures do not compromise neurons' electroactivity. Imaging results for the co-cultures showed that the spontaneous firing rate is higher for rat neurons growing directly on top of the astrocytes than for those growing inside the pillar cavities without ramps (Fig. 7c). The rat neurons growing directly on top of the astrocytes also showed significantly increased firing rate compared to monoculture firing rates, indicating that rat astrocytes promote the maturation of electrophysiological signals when in direct contact with the neurons (Fig. S6 in the Supplementary Material). Interestingly, the addition of the ramp connectors showed no increase in firing rate for the neurons with neurite connections to the co-culture on the glass substrate compared to those growing in the pillars without ramps. This result indicates that the contact provided by neurite extensions is insufficient to provide the increased maturation effect observed when neurons and astrocytes are in direct contact.

Overall, the presented 3D-printed neurite-guidance co-culture platform allowed us to investigate in detail how the electrophysiological properties of neurons are affected by astrocytes. Only direct cell-body contact between rat neurons and astrocytes affects the neurons, whereas chemical signaling or contact through neurites does not show any effects. This new insight would not have been observable using previously described co-culture methods.

## 3. Conclusion

We have demonstrated that 3D printing with the readily available IP-Visio resin can create contact and non-contact 3D co-cultures with micrometer precision, allowing live high-spatial and temporal resolution fluorescent imaging. We achieved a neurite guidance co-culture model of neurons and astrocytes with spatial localization of the astrocytes with a simple and completely scalable seeding method. The non-cytotoxic and low-autofluorescence properties of the resin allowed for immunocytochemistry-based protein expression analysis and calcium signal imaging as a direct non-contact method to assess neuronal electrophysiology. Viability assay and protein expression analysis of LUHMES cells in co-culture with human fetal cortical astrocytes showed that this glial cell type could not support the maturation of LUHMES cells towards a neuronal phenotype. Further, calcium signaling analysis with rat neurons and astrocytes revealed that direct cell-body contact between neurons and astrocytes results in increased neuronal calcium activity,

whereas cell-projection contact does not affect the calcium transients. The presented platform can enable multi-well arrays with the optical readout of co-culture models for functional studies of neural activity and processes relevant to neurological disorders.

## 4. Experimental section

### 4.1. Substrates, materials, and reagents for sample preparation

Soda-lime glass slides (L x W x T: 25 mm × 25 mm x 0.7 mm) coated with indium tin oxide (ITO, around 18 nm thick, 100–300 Ohm/square) were purchased as printing substrates from Nanoscribe (Germany). Acetone (product number 5048858, VWR), isopropanol (product number 20839.366, VWR), and deionized water (DI water, purified from tap water by a Milli-Q® Type I direct water purification system, Merck) were used to clean the substrates. A 1:200 v/v solution of siloxane (3-(trimethoxysilyl)propyl methacrylate, product number M6514, Sigma Aldrich) in 96% Ethanol (product number 20823.362, VWR) was used to increase the adhesion of the 3D printed resin to the ITO-coated glass substrates, as described in the silanization section. For the 3D printing process, IP-Visio resin (Nanoscribe proprietary resin based on 7, 7, 9(or 7, 9, 9)-trimethyl-4, 13-dioxo-3, 14-dioxa-5, 12-diazahexadecane-1, 16-diyl bismethacrylate, CAS No. 72869-86-4; full formulation listed in Table S2 in the Supplementary Material) and propylene glycol methyl ether acetate (PGMEA, product number 484431, Sigma-Aldrich) were used as two-photon printable resin and developer, respectively.

### 4.2. Substrate cleaning and silanization

The substrates were first cleaned by subsequent submersions of the substrates in acetone, isopropanol, and DI water. Then, to make the silanization more effective, the ITO-coated surface of the glass substrates was activated by oxygen plasma treatment in a plasma chamber (FEMTO, Diener electronic) using 40 W power, 1 mbar process pressure, and 800 cm$^3$/min of air gas flow. After oxygen plasma activation, the substrates were submerged in a prepared solution of 3-(trimethoxysilyl)propyl methacrylate in 96% ethanol (1:200 vol ratio) overnight, keeping the ITO-coated side facing upwards during the treatment. The substrates were then rinsed with acetone and deionized water, and blown dry with air. Finally, the functionalized samples were transferred into a petri dish,

sealed with parafilm (product number P7793-1 EA, Sigma-Aldrich), and used for printing within 72 h.

### 4.3. Design choice for the 3D platform

A 3D CAD model of interconnected pillars was designed using SolidWorks software (Dassault Systèmes) and transformed into a Nanoscribe print design using the proprietary software Describe (Nanoscribe). The designed 3D platform comprised two arrays of $4 \times 2$ pillars connected by suspended bridges (Fig. 2a). Each array consisted of 150 μm high square-based pillars with 140 μm long edges and a 50 μm deep cavity on top of the pillar to host the neurons and prevent them from migrating to other areas after cell seeding and adhesion (Fig. 2b). The pillars were connected to each other by 250-μm-long suspended bridges that serve as guiding structures for the neurites to form a network on top of the printed structures. The suspended bridges were 30 μm thick and 25 μm wide and had a guiding cavity 15 μm deep and 10 μm wide. We designed the pillar array design described above to allow the study of neurons on the printed structure, separated from the substrate plane. We also included a second pillar array design to create specific pathways for physical contact between the neurons inside the pillar cavities and the co-culture of neurons and astrocytes on the underlying substrate. The design was identical to the first pillar array except for 45-degree ramps connecting the pillar cavities and substrate plane (Fig. 2a, right).

### 4.4. Optimization of the laser exposure parameters for two-photon polymerization direct writing

We optimized the pattern fidelity by printing an array of 50-μm-edge cubes with pulse energies and scanning speeds ranging from 420 pJ to 730 pJ and from 70 mm/s to 120 mm/s, respectively. To minimize processing time, the hatching and slicing distance values were expanded from the recommended values of 0.5 μm and 1 μm–0.55 μm and 1.1 μm, respectively. The optimized pulse energy and speed parameters (730 pJ and 70 mm/s) were then used to expose the IP Visio resin and print the 3D structures for cell seeding.

### 4.5. Structure printing and development

3D polymeric structures were printed using a two-photon 3D printer (Photonic Professional GT2, Nanoscribe) with low fluorescence and the non-cytotoxic (according to ISO 10993-5/USP 87) Nanoscribe resin IP-Visio. The IP-Visio resin was applied at room temperature onto functionalized ITO-coated glass slides and exposed in immersion configuration using a 25x objective (Objective LCI Plan-Neofluar 25x/0.8 Imm Corr DIC M27, product number 420852-9972-000, Zeiss). The two-photon printer used a laser beam at 780 nm wavelength, a pulse duration of around 100 fs, and a repetition rate of 80 MHz. After printing, the samples were submerged in PGMEA for 20 min, then transferred into isopropanol for 5 min. To increase the degree of crosslinking, post-print curing via UV-driven radical generation was performed (3 min, 220–450 nm wavelength, 10 mW/cm$^2$) using an OAI Model 30 UV Light Source. Next, the samples were transferred to DI water at 65 °C for 10 min to facilitate the desorption of unreacted species and solvents. Then, the samples were carefully dried, avoiding air blowing on top of the printed structures to prevent possible mechanical damage and delamination. Finally, the dried samples were transferred to a petri dish, sealed with parafilm, and stored at room temperature until cell seeding.

### 4.6. Characterization of the 3D printed structures by scanning electron microscopy (SEM)

SEM was used to optimize the printing parameters (processing speed and laser pulse energy) and assess post-printing shrinkage. The printed structures were metalized by sputtering approximately 50 nm of gold with a 10-nm thick adhesion layer of TiW alloy (KDF 844NT batch sputtering system, KDF Inc.) and imaged using a scanning electron microscope (SEM, Carl Zeiss AG - ULTRA 55, Carl Zeiss, Germany).

### 4.7. Device preparation for cell seeding

To reduce the volume of necessary reagents and cells, a polydimethylsiloxane (PDMS) ring was attached to the glass substrates to create a cell culture well with the structures in its center. PDMS and its curing agent (Sylgard 184 Silicone Elastomer Kit, Dow) were mixed at a weight ratio of 10:1, degassed, and hardened in a petri dish at 70 °C for a minimum of 3 h. The resulting PDMS slab with a thickness of 5 mm was punched using a 10 mm biopsy punch and trimmed on the side with a scalpel to fit on top of the glass slide. The PDMS ring was then placed on top of the glass surface. The samples were sterilized by soaking them in 70% ethanol for 5 min and then rinsed two times with DI water and Dulbecco's phosphate buffered saline (DPBS product number 14190144, Gibco). Finally, samples were coated with 160 μg/mL growth-factor-reduced Matrigel® (product number 354230, Corning) in DPBS overnight at 37 °C. The coating solution was washed with cell media before cell seeding. It is also possible to reuse the printed samples after the cell culture experiment, leaving them in 0.5% Alconox® detergent solution (product number 560437Q, VWR) overnight at RT and washing them three times with water and DPBS before use.

### 4.8. Cell culture

Human astrocytes (product number 1800, ScienCell) were cultivated in Astrocyte Media (AM, product number 1801, ScienCell) supplemented with 2% (v/v) fetal bovine serum (FBS, product number 0010, ScienCell), 1% of astrocyte growth supplement (AGS, product number 1852, ScienCell) and 1% penicillin/streptomycin (P/S, product number 0503, ScienCell). Astrocytes were expanded in tissue culture treated flasks with media changes every second day, passaged when 90% confluent using TrypLE Select (product number 12563011, Gibco), and always used at passage 6 for seeding in the devices. Conditionally immortalized proliferating Lund human mesencephalic (LUHMES, product number T0284, abm) cells were cultivated and differentiated according to the protocol by Scholz et al. with minor modifications in the optimized co-culture protocol (described at the end of this section). [33] Tissue culture treated flasks (T25) were coated by incubating them in a solution of 50 μg/mL poly-L-ornithine hydrobromide (PLO, product number P3655, Merck) and 1 μg/mL human plasma fibronectin (product number FC010, Merck) in DI water (product number 10977035, Invitrogen) overnight at 37 °C. After removing the coating solution, the flasks were washed with DI water and left to dry for 5 min at room temperature before cell seeding. LUHMES cells were grown in Advanced Dulbecco's modified Eagle's medium/F12 (Adv-DMEM/F12, product number 12634010, Gibco) supplemented with 1x N2 (product number 17502-048, Gibco), 2 mM L-glutamine (product number 25030024, Thermo Scientific), and 40 ng/mL recombinant human fibroblast growth factor (FGF, product number 233-FB, R&D Systems) at 37 °C and 5% $CO_2$. Cells were passaged 1:10 when reaching 80%–90% confluency. For differentiation, LUHMES cells were seeded on coated T25 flasks at a density of 46′000 cells/cm$^2$ in growth media. After 24 h (Differentiation Day 0, or DD0), the media formulation was changed to differentiation media, consisting of Adv-DMEM/F12 supplemented with 1xN2, 2 mM L-glutamine, 1 mM diburtyryl cAMP (product number S7858, Selleck Chemicals), 1 μg/mL tetracycline (product number T7660, Merck) and 2 ng/mL recombinant human GDNF (product number 450-10, PeproTech). After two days (DD2), pre-differentiated LUHMES cells were passaged using TrypLE Select and reseeded at a density of 150′000 cells/cm$^2$ on the selected substrate to finish the differentiation. Half the culture media was changed every three days until the desired endpoint.

For the co-culture experiments with human astrocytes and LUHMES, human astrocytes were seeded on pre-coated samples in astrocyte media at a density of 2500 cells/cm$^2$ one day before starting the differentiation

protocol for the LUHMES cells (Differentiation Day -1, or DD-1). Astrocyte media was replaced once after two days (DD1). After three days (DD2), the astrocyte media was replaced by the LUHMES differentiation media, and pre-differentiated LUHMES cells were seeded on top of the human astrocytes at a density of 150000 cells/cm$^2$. Co-cultures were then kept in the LUHMES differentiation media with half media changes every three days until the endpoint of the experiment. In the optimized co-culture protocol (DM+), pre-differentiated LUHMES cells were seeded on top of the astrocytes at a density of 60′000 cells/cm$^2$, the LUHMES differentiation media was supplemented with additional 1% of AGS and 10 μM ROCK inhibitor (Y-27632 Dihydrochloride, product number 72304, Stemcell Technologies) for the first three days of co-culture (DD 2–5) followed by LUHMES differentiation media supplemented with 1% AGS without ROCK inhibitor (DD5). Further, half-media changes were performed every three days until the endpoint of the experiment. The seeding density was reduced in the optimized media condition to obtain the same final density of differentiated cells.

For the co-culture experiments with rat astrocytes and neurons, primary cortical rat astrocytes (product number N7745100, Gibco) were cultivated according to the suggested protocol provided by Thermo-Fisher. Rat astrocytes were expanded in DMEM high glucose (product number 11995065, Gibco) with 15% FBS (product number 16000-036, Gibco) and 1% P/S in tissue culture treated flasks. At the third cell passage, the rat astrocytes were seeded on pre-coated samples at a density of 2500 cells/cm$^2$. After four days, Primary Rat Cortex Neurons (product number A1084001, Gibco) were thawed up and seeded on top of the rat astrocytes at a density of 75′000 viable cells/cm$^2$ in Neurobasal Plus media (product number A3582901, Gibco) supplemented with 0.5 mM Glutamax (product number 35050-038, Thermo Scientific), 2% B-27 supplement (product number 17504044, Gibco) and 1% P/S. Half media changes were performed every three days. For increased viability of the rat neurons, the optimized media was supplemented with 1% AGS and 10 μM ROCK inhibitor for the first three days, followed by media supplemented with 1% AGS until the endpoint of the experiment (red data points in Fig. 7 S5).

### 4.9. Immunocytochemistry

Cell samples were fixed at a final concentration of 4% low methanol formaldehyde solution (product number 4235.4, Roth). Samples were then incubated in blocking buffer (DPBS with 10% goat serum, product number G923, Merck, and 0.1% Triton X-100, product number HFH10, Invitrogen) for 1 h. Primary antibodies were incubated in dilution buffer (DPBS with 1% goat serum and 0.01% Triton X-100) overnight at 4 °C. Secondary antibodies were incubated in the dilution buffer for 1 h at room temperature. Nuclear staining was performed with Hoechst (1:2000 in dilution buffer) for 10 min. After each incubation step, the samples were washed three times with DPBS. The following antibodies were used: anti-TUBB3 (1:500, product number 801201, Biolegend), anti-TH (1:500, product number P40101, PelFreez), anti SYN1 (1:500, product number AB1543, Merck), anti DCX (1:800, product number 4604S, Cell Signalling), anti-rabbit Alexa Fluor 488 (1:1000, product number A21206, Invitrogen), anti-rabbit CF594 (1:1000, product number SAB4600107, Merck) and CF633 anti-mouse (1:1000, product number A-21136, Invitrogen). A Nikon CrEST X-light V3 spinning disc was used to image the samples.

### 4.10. Live Imaging

For the cell tracker experiments, astrocytes and LUHMES cells were incubated, respectively, with green cell tracker CMFDA (10 μM, product number C7025, Invitrogen) and red cell tracker CMTPX (10 μM, product number C34552, Invitrogen) for 30 min in PBS at 37 °C with 5% CO$_2$ and then washed three times with cell culture media. For the image series in Fig. 4, the astrocytes were re-stained just before seeding LUHMES cells to obtain a stronger fluorescent signal to counter the dilution of the

fluorophore due to the proliferation of the astrocytes. The green and red colors of the dyes were replaced in Fig. 4 with a blue/red colorblindness-friendly palette. For the calcium imaging, cells were incubated in 0.75 μM Calbryte™ 520 AM (AAT Bioquest, product number 2065) for 45 min at 37 °C and washed three times with respective cell media before the experiment. For the live/DEAD assay, we used a Viability/Cytotoxicity Kit (product number L23224, Invitrogen). Samples were incubated in a final concentration of 2 μM calcein AM and 4 μM Ethidium homodimer-1 in PBS for 30 min at RT. All live imaging was performed with a Zeiss Cell Observer microscope equipped with an incubator chamber, heating, CO$_2$ control, and a Zeiss AxioCam MRm camera.

### 4.11. Imaging analysis

We used IMARIS image processing software to perform the live/dead and protein expression analysis. For the live-dead quantification, live-&dead cells were defined and counted using the spot function (⌀ = 10 μm). For the gene expression analysis, nuclei were counted using the spot function (⌀ = 10 μm), and we used the surface function to quantify the expression of the TH, DCX, and SYN1. The determined area of the expressed protein was normalized to the number of cells. For the calcium imaging analysis, randomly selected cells were marked in FIJI to plot the fluorescent intensity change over time and count the total spikes. Only cells inside the pillar cavities were analyzed, while the cells attached to the outer side of the printed pillar structure were excluded from the count and analysis.

### 4.12. Statistical analysis

Origin Pro was used to calculate p-values using ANOVA, two-sample t-tests, and Linear Mixed Models.

**Credit author statement**

**Sebastian Buchmann:** Conceptualization (Supporting); Data curation (Leading); Formal analysis (Leading); Investigation (Leading); Methodology (Equal); Validation (Leading); Visualization (Equal); Roles/Writing - original draft (Supporting); Writing - review & editing (Supporting). **Alessandro Enrico:** Conceptualization (Leading); Data curation (Supporting); Formal analysis (Supporting); Investigation (Supporting); Methodology (Equal); Validation (Supporting); Visualization (Equal); Roles/Writing - original draft (Leading); Writing - review & editing (Leading). **Muriel Alexandra Holzreuter:** Data curation (Supporting); Formal analysis (Supporting); Investigation (Supporting); Methodology (Supporting). **Michael Reid:** Data curation (Supporting); Formal analysis (Supporting); Investigation (Supporting); Methodology (Supporting); Software (Supporting); Validation (Supporting); Visualization (Supporting). **Erica Zeglio:** Roles/Writing - original draft (Supporting); Writing - review & editing (Supporting). **Frank Niklaus:** Conceptualization (Supporting); Funding acquisition (Equal); Methodology (Supporting); Project administration (Supporting); Resources (Supporting); Supervision (Supporting); Roles/Writing - original draft (Supporting); Writing - review & editing (Supporting). **Göran Stemme:** Conceptualization (Supporting); Funding acquisition (Equal); Methodology (Supporting); Project administration (Supporting); Resources (Supporting); Supervision (Supporting); Roles/Writing - original draft (Supporting); Writing - review & editing (Supporting). **Anna Herland:** Conceptualization (Supporting); Formal analysis (Supporting); Methodology (Supporting); Funding acquisition (Equal); Project administration (Leading); Resources (Leading); Supervision (Leading); Roles/Writing - original draft (Supporting); Writing - review & editing (Supporting).

## Declaration of competing interest

## Data availability

Data will be made available on request.

## Acknowledgments

## Appendix A. Supplementary data

Supplementary data to this article can be found online at https://doi.org/10.1016/j.mtbio.2023.100706.

## References

[1] P.M. Holloway, S. Willaime-Morawek, R. Siow, M. Barber, R.M. Owens, A.D. Sharma, W. Rowan, E. Hill, M. Zagnoni, Advances in microfluidic in vitro systems for neurological disease modeling, J. Neurosci. Res. 99 (2021) 1276–1307, https://doi.org/10.1002/jnr.24794.

[2] C. Jensen, Y. Teng, Is it time to start transitioning from 2D to 3D cell culture? Front. Mol. Biosci. 7 (2020) 33, https://doi.org/10.3389/fmolb.2020.00033.

[3] E.G.Z. Centeno, H. Cimarosti, A. Bithell, 2D versus 3D human induced pluripotent stem cell-derived cultures for neurodegenerative disease modelling, Mol. Neurodegener. 13 (2018), https://doi.org/10.1186/s13024-018-0258-4.

[4] P. Nikolakopoulou, R. Rauti, D. Voulgaris, I. Shlomy, B.M. Maoz, A. Herland, Recent progress in translational engineered in vitro models of the central nervous system, Brain 143 (2021) 3181–3213, https://doi.org/10.1093/BRAIN/AWAA268.

[5] A. Birgersdotter, R. Sandberg, I. Ernberg, Gene expression perturbation in vitro - a growing case for three-dimensional (3D) culture systems, Semin. Cancer Biol. 15 (2005) 405–412, https://doi.org/10.1016/j.semcancer.2005.06.009.

[6] C.C. Dufort, M.J. Paszek, V.M. Weaver, Balancing forces: architectural control of mechanotransduction, Nat. Rev. Mol. Cell Biol. 12 (2011) 308–319, https://doi.org/10.1038/nrm3112.

[7] A. Wolff, M. Antfolk, B. Brodin, M. Tenje, Vitro blood-brain barrier models - an overview of established models and new microfluidic approaches, J. Pharmaceut. Sci. 104 (2015) 2727–2746, https://doi.org/10.1002/jps.24329.

[8] S.H. Lee, K.Y. Shim, B. Kim, J.H. Sung, Hydrogel-based three-dimensional cell culture for organ-on-a-chip applications, Biotechnol. Prog. 33 (2017) 580–589, https://doi.org/10.1002/btpr.2457.

[9] S. Zhang, Z. Wan, R.D. Kamm, Vascularized organoids on a chip: strategies for engineering organoids with functional vasculature, Lab Chip 21 (2021) 473–488, https://doi.org/10.1039/d0lc01186j.

[10] A. Enrico, D. Voulgaris, R. Östmans, N. Sundaravadivel, L. Moutaux, A. Cordier, F. Niklaus, A. Herland, G. Stemme, 3D microvascularized tissue models by laser-based cavitation molding of collagen, Adv. Mater. 34 (2022), 2109823, https://doi.org/10.1002/adma.202109823.

[11] E. Neto, L. Leitão, D.M. Sousa, C.J. Alves, I.S. Alencastre, P. Aguiar, M. Lamghari, Compartmentalized microfluidic platforms: the unrivaled breakthrough of in vitro tools for neurobiological research, J. Neurosci. 36 (2016) 11573–11584, https://doi.org/10.1523/JNEUROSCI.1748-16.2016.

[12] I. Matthiesen, D. Voulgaris, P. Nikolakopoulou, T.E. Winkler, A. Herland, Continuous monitoring reveals protective effects of N-acetylcysteine amide on an isogenic microphysiological model of the neurovascular unit, Small 17 (2021), 2101785, https://doi.org/10.1002/SMLL.202101785.

[13] D. Pamies, T. Hartung, H.T. Hogberg, Biological and medical applications of a brain-on-a-chip, Exp. Biol. Med. 239 (2014) 1096–1107, https://doi.org/10.1177/1535370214537738.

[14] Z. Tong, M. Segura-Feliu, O. Seira, A. Homs-Corbera, J.A. Del Río, J. Samitier, A microfluidic neuronal platform for neuron axotomy and controlled regenerative studies, RSC Adv. 5 (2015) 73457–73466, https://doi.org/10.1039/c5ra11522a.

[15] H. Kavand, R. Nasiri, A. Herland, Advanced materials and sensors for microphysiological systems: focus on electronic and electrooptical interfaces, Adv. Mater. 34 (2022), 2107876, https://doi.org/10.1002/adma.202107876.

[16] M.J.J. Van Velthoven, R. Ramadan, F.S. Zügel, B.J. Klotz, D. Gawlitta, P.F. Costa, J. Malda, M.D. Castilho, L.M.O. De Kort, P. De Graaf, Gel casting as an approach for tissue engineering of multilayered tubular structures, Tissue Eng. C Methods 26 (2020) 190–198, https://doi.org/10.1089/ten.tec.2019.0280.

[17] J.H. Choi, H. Lee, H.K. Jin, J.S. Bae, G.M. Kim, Fabrication of microengineered templates and their applications into micropatterned cell culture, J. Biomed. Nanotechnol. 9 (2013) 377–381, https://doi.org/10.1166/JBN.2013.1508.

[18] M.T. Calejo, J. Saari, H. Vuorenpää, E. Vuorimaa-Laukkanen, P. Kallio, K. Aalto-Setälä, S. Miettinen, H. Skottman, M. Kellomäki, K. Juuti-Uusitalo, Co-culture of human induced pluripotent stem cell-derived retinal pigment epithelial cells and endothelial cells on double collagen-coated honeycomb films, Acta Biomater. 101 (2020) 327–343, https://doi.org/10.1016/j.actbio.2019.11.002.

[19] L.A. Bruggeman, R.P. Doan, J. Loftis, A. Darr, A. Calabro, A cell culture system for the structure and hydrogel properties of basement membranes: application to capillary walls, in: Cell. Mol. Bioeng., Springer, 2012, pp. 194–204, https://doi.org/10.1007/s12195-012-0221-3.

[20] S. Taqvi, K. Roy, Influence of scaffold physical properties and stromal cell coculture on hematopoietic differentiation of mouse embryonic stem cells, Biomaterials 27 (2006) 6024–6031, https://doi.org/10.1016/j.biomaterials.2006.05.052.

[21] Z. Zheng, D. Eglin, M. Alini, G.R. Richards, L. Qin, Y. Lai, Visible light-induced 3D bioprinting technologies and corresponding bioink materials for tissue engineering: a review, Engineering 7 (2021) 966–978, https://doi.org/10.1016/j.eng.2020.05.021.

[22] A.M. Taylor, M. Blurton-Jones, S.W. Rhee, D.H. Cribbs, C.W. Cotman, N.L. Jeon, A microfluidic culture platform for CNS axonal injury, regeneration and transport, Nat. Methods 2 (2005) 599–605, https://doi.org/10.1038/nmeth777.

[23] Z. Tong, E. Kwak, A. Aguiar, B. Peng, C.W. Pouton, N.H. Voelcker, J.M. Haynes, Compartmentalized microfluidic chambers enable long-term maintenance and communication between human pluripotent stem cell-derived forebrain and midbrain neurons, Lab Chip 21 (2021) 4016–4030, https://doi.org/10.1039/d1lc00505g.

[24] S. Girardin, B. Clément, S.J. Ihle, S. Weaver, J.B. Petr, J.C. Mateus, J. Duru, M. Krubner, C. Forró, T. Ruff, I. Fruh, M. Müller, J. Vörös, Topologically controlled circuits of human iPSC-derived neurons for electrophysiology recordings, Lab Chip 22 (2022) 1386–1403, https://doi.org/10.1039/d1lc01110c.

[25] C. Fendler, C. Denker, J. Harberts, P. Bayat, R. Zierold, G. Loers, M. Münzenberg, R.H. Blick, Microscaffolds by direct laser writing for neurite guidance leading to tailor-made neuronal networks, Adv. Biosyst. 3 (2019), 1800329, https://doi.org/10.1002/adbi.201800329.

[26] R. Zierold, J. Harberts, C. Fendler, J. Teuber, M. Siegmund, A. Silva, N. Rieck, M. Wolpert, R.H. Blick, Toward brain-on-a-chip: human induced pluripotent stem cell-derived guided neuronal networks in tailor-made 3d nanoprinted microscaffolds, ACS Nano 14 (2020) 13091–13102, https://doi.org/10.1021/acsnano.0c04640.

[27] A. Accardo, M.C. Blatché, R. Courson, I. Loubinoux, C. Thibault, L. Malaquin, C. Vieu, Multiphoton direct laser writing and 3D imaging of polymeric freestanding architectures for cell colonization, Small 13 (2017), 1700621, https://doi.org/10.1002/smll.201700621.

[28] M. Schmid, D. Ludescher, H. Giessen, Optical properties of photoresists for femtosecond 3D printing: refractive index, extinction, luminescence-dose dependence, aging, heat treatment and comparison between 1-photon and 2-photon exposure, Opt. Mater. Express 9 (2019) 4564, https://doi.org/10.1364/ome.9.004564.

[29] M. Hasan, S. Blair, Maximizing transmittance in two-photon 3D printed materials for micro-optics in the visible, Opt. Mater. Express 12 (2022) 895, https://doi.org/10.1364/ome.448819.

[30] M.S. Reid, A. Träger, C. Cobo Sanchez, E. Malmström, L. Wågberg, Tunable adhesion and interfacial structure of layer-by-layer assembled block co-polymer micelle and polyelectrolyte coatings, Adv. Mater. Interfac. (2022), 2200065, https://doi.org/10.1002/ADMI.202200065.

[31] J. Purtov, A. Verch, P. Rogin, R. Hensel, Improved development procedure to enhance the stability of microstructures created by two-photon polymerization, Microelectron. Eng. 194 (2018) 45–50, https://doi.org/10.1016/j.mee.2018.03.009.

[32] X. Zhou, Y. Hou, J. Lin, A review on the processing accuracy of two-photon polymerization, AIP Adv. 5 (2015), 030701, https://doi.org/10.1063/1.4916886.

[33] D. Scholz, D. Pöltl, A. Genewsky, M. Weng, T. Waldmann, S. Schildknecht, M. Leist, Rapid, complete and large-scale generation of post-mitotic neurons from the human LUHMES cell line, J. Neurochem. 119 (2011) 957–971, https://doi.org/10.1111/j.1471-4159.2011.07255.x.

[34] X.M. Zhang, M. Yin, M.H. Zhang, Cell-based assays for Parkinson's disease using differentiated human LUHMES cells, Acta Pharmacol. Sin. 35 (2014) 945–956, https://doi.org/10.1038/aps.2014.36.

[35] L. Smirnova, G. Harris, J. Delp, M. Valadares, D. Pamies, H.T. Hogberg, T. Waldmann, M. Leist, T. Hartung, A LUHMES 3D dopaminergic neuronal model for neurotoxicity testing allowing long-term exposure and cellular resilience analysis, Arch. Toxicol. 90 (2016) 2725–2743, https://doi.org/10.1007/s00204-015-1637-z.

[36] L. Efremova, S. Schildknecht, M. Adam, R. Pape, S. Gutbier, B. Hanf, A. Bürkle, M. Leist, Prevention of the degeneration of human dopaminergic neurons in an astrocyte co-culture system allowing endogenous drug metabolism, Br. J. Pharmacol. 172 (2015) 4119–4132, https://doi.org/10.1111/bph.13193.

[37] S. Gutbier, A.S. Spreng, J. Delp, S. Schildknecht, C. Karreman, I. Suciu, T. Brunner, M. Groettrup, M. Leist, Prevention of neuronal apoptosis by astrocytes through thiol-mediated stress response modulation and accelerated recovery from proteotoxic stress, Cell Death Differ. 25 (2018) 2101–2117, https://doi.org/10.1038/s41418-018-0229-x.

[38] L. Efremova, P. Chovancova, M. Adam, S. Gutbier, S. Schildknecht, M. Leist, Switching from astrocytic neuroprotection to neurodegeneration by cytokine stimulation, Arch. Toxicol. 91 (2017) 231–246, https://doi.org/10.1007/s00204-016-1702-2.

[39] C.J. Hindley, A.L. Condurat, V. Menon, R. Thomas, L.M. Azmitia, J.A. Davis, J. Pruszak, The Hippo pathway member YAP enhances human neural crest cell fate and migration, Sci. Rep. 6 (2016) 1–9, https://doi.org/10.1038/srep23208.

[40] A. Gaceb, M. Barbariga, G. Paul, An in vitro partial lesion model of differentiated human mesencephalic neurons: effect of pericyte secretome on phenotypic markers, J. Mol. Neurosci. 70 (2020) 1914–1925, https://doi.org/10.1007/s12031-020-01589-6.

[41] F. Yang, Y. Liu, J. Tu, J. Wan, J. Zhang, B. Wu, S. Chen, J. Zhou, Y. Mu, L. Wang, Activated astrocytes enhance the dopaminergic differentiation of stem cells and promote brain repair through bFGF, Nat. Commun. 5 (2014) 1–14, https://doi.org/10.1038/ncomms6627.

[42] F. Du, Q. Yu, A. Chen, D. Chen, S. ShiDu Yan, Astrocytes attenuate mitochondrial dysfunctions in human dopaminergic neurons derived from iPSC, Stem Cell Rep. 10 (2018) 366–374, https://doi.org/10.1016/j.stemcr.2017.12.021.

[43] I. Datta, K. Ganapathy, R. Razdan, R. Bhonde, Location and number of astrocytes determine dopaminergic neuron survival and function under 6-OHDA stress

[44] N.S. Roy, C. Cleren, S.K. Singh, L. Yang, M.F. Beal, S.A. Goldman, Functional engraftment of human ES cell-derived dopaminergic neurons enriched by coculture with telomerase-immortalized midbrain astrocytes, Nat. Med. 12 (2006) 1259–1268, https://doi.org/10.1038/nm1495.

[45] K.A. Buytaert-Hoefen, E. Alvarez, C.R. Freed, Generation of tyrosine hydroxylase positive neurons from human embryonic stem cells after coculture with cellular substrates and exposure to GDNF, Stem Cell. 22 (2004) 669–674, https://doi.org/10.1634/stemcells.22-5-669.

[46] B.J. Kim, J.Y. Choi, H. Choi, S. Han, J. Seo, J. Kim, S. Joo, H.M. Kim, C. Oh, S. Hong, P. Kim, I.S. Choi, Astrocyte-encapsulated hydrogel microfibers enhance neuronal circuit generation, Adv. Healthc. Mater. 9 (2020), 1901072, https://doi.org/10.1002/adhm.201901072.

[47] L.E. Clarke, B.A. Barres, Emerging roles of astrocytes in neural circuit development, Nat. Rev. Neurosci. 14 (2013) 311–321, https://doi.org/10.1038/nrn3484.

[48] X. Tang, L. Zhou, A.M. Wagner, M.C.N. Marchetto, A.R. Muotri, F.H. Gage, G. Chen, Astroglial cells regulate the developmental timeline of human neurons differentiated from induced pluripotent stem cells, Stem Cell Res. 11 (2013) 743–757, https://doi.org/10.1016/j.scr.2013.05.002.

[49] J. Kuijlaars, T. Oyelami, A. Diels, J. Rohrbacher, S. Versweyveld, G. Meneghello, M. Tuefferd, P. Verstraelen, J.R. Detrez, M. Verschuuren, W.H. De Vos, T. Meert, P.J. Peeters, M. Cik, R. Nuydens, B. Brône, A. Verheyen, Sustained synchronized neuronal network activity in a human astrocyte co-culture system, Sci. Rep. 6 (2016) 1–14, https://doi.org/10.1038/srep36529.

[50] A. Ahtiainen, B. Genocchi, J.M.A. Tanskanen, M.T. Barros, J.A.K. Hyttinen, K. Lenk, Astrocytes exhibit a protective role in neuronal firing patterns under chemically induced seizures in neuron–astrocyte co-cultures, Int. J. Mol. Sci. 22 (2021), 12770, https://doi.org/10.3390/ijms222312770.